ON THE IMPORTANCE OF VALIDATION WHEN USING COMMERCIAL CFD CODES IN NUCLEAR REACTOR SAFETY

Heinz Wilkening[a], Daniele Baraldi[a] and Matthias Heitsch[b]

[a] Institute for Energy, DG Joint Research Centre, European Commission, Petten, The Netherlands

[b] Gesellschaft für Anlagen- und Reaktorsicherheit GRS (mbH), Köln, Germany

Abstract

In this validation work two turbulence models (k-ε and SST model) and two grids (a finer hybrid grid and a tetrahedral coarser grid) are considered in order to model helium release and dispersion. Simulation results are compared against an experiment of jet release phenomena in the Battelle Model Containment facility (BMC), a multi-compartment facility with a total volume of about 560 m^3. In the selected test, HYJET Jx7, helium was released into the containment at a speed of 42 m/s over a time of 200 s. Although the k-ε model is the most commonly used turbulence model in most CFD applications, it does not provide the most accurate predictions for this application. Alternatively the SST turbulence model has been employed giving more accurate results. This investigation provides a confirmation that the validation of commercial CFD codes is always required in order to select the more suitable physical models and computational grids for each specific application.

1 Introduction

CFD (Computational Fluid Dynamics) simulations are playing an increasingly important role in safety analysis for nuclear applications. This trend is driven by the fact that experiments, especially at large scale, are very costly and often not feasible. Moreover the ever-increasing speed of today's high performance computer is making possible to perform CFD simulations of realistic scenarios. Initially the CFD codes used in nuclear reactor safety were mostly in-house research codes developed for a dedicated purpose. Similarly, at JRC we have developed our own CFD code REACFLOW for simulations of hydrogen explosions during a severe nuclear accident. In more recent times users have also the choice to use commercial multi-purpose CFD codes. These codes have a wide range of application especially in the non-nuclear field, such as aerodynamics, turbo-machinery, automotive and so on. Typically commercial codes have been validated by the suppliers. Nevertheless when a user applies a commercial CFD code to a specific problem, he/she has to make several choices in the generation of the computational mesh and in the selection of the physical models. One challenging problem in CFD analysis is the modelling of turbulent flows. Up to now there is no universal turbulence model that is suitable for all applications. Therefore commercial CFD codes offer a wide range of turbulence models to choose from. The choice should depend only on the physics of the problem. Nevertheless the user should be aware that his choice has several implications e.g. also on the computational grid to be used.

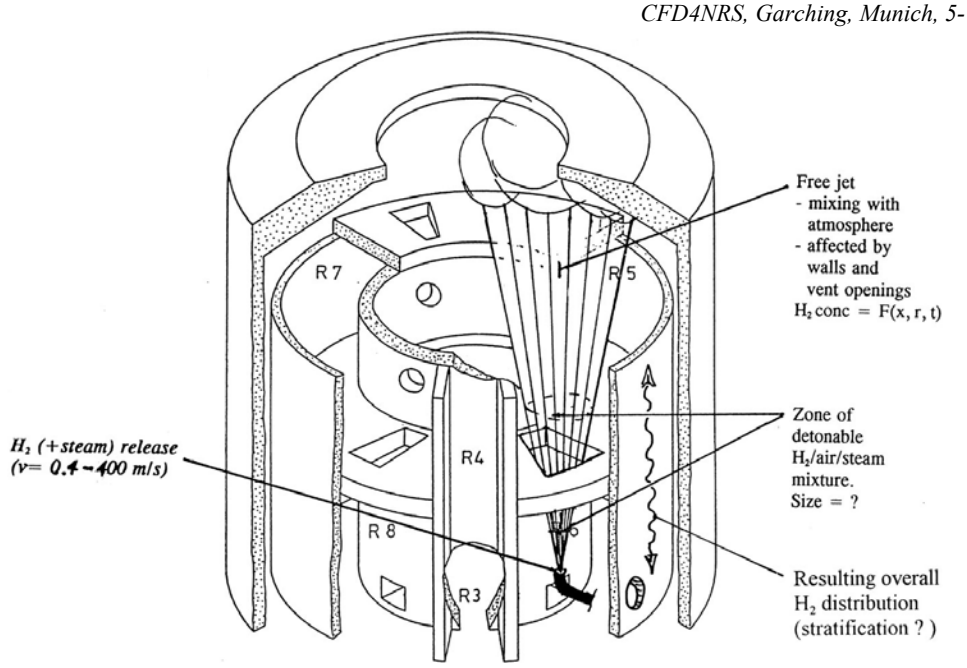

Figure 1: Battelle Model Containment in the HYJET configuration

The commercial CFD code CFX from ANSYS was selected to model hydrogen release and mixing in nuclear reactor containments. The release of hydrogen could occur in a severe accident when hydrogen is produced in large quantities during the core melt down. To understand the hydrogen dispersion process is extremely important as the hydrogen distribution describes the initial conditions for the potential hydrogen explosion within the containment. The strength of the explosion depends strongly on the initial hydrogen distribution. The explosion could jeopardise the containments integrity and cause a release of radioactivity into the environment. The physical processes of main interest in gas-dispersion are turbulent transport and mixing, buoyancy and condensation.

The validation work presented hereafter is focussing on the turbulence model to be chosen for modelling hydrogen release. Two turbulence models (k-ε and SST model) and two grids (a finer grid with a hybrid mesh near walls and a coarser grid - only tetrahedral) are considered in the analysis. Simulation results are compared against an experiment of jet release phenomena in the Battelle Model Containment facility (BMC), a multi-compartment facility with a total volume of about 560 m^3. In the selected test, HYJET Jx7, helium was released into the containment at a speed of 42 m/s over a time of 200 s. Because of safety concerns, replacing hydrogen with helium is a standard procedure in experiments whose aim is to investigate the behaviour of large masses of light gasses.

2. Validation Experiment

The Battelle Model Containment (BMC) was built at Battelle Ingenieurtechnik GmbH, Frankfurt am Main, Germany, as a purpose-built test facility for short- and medium-term LOCA (Loss of Coolant Accident) investigations in 1972/73. In its original configuration the test facility consisted of a 5 m^3 high-pressure system and a compartmentalised 600 m^3 containment building of unlined concrete, in a linear 1:4 scale compared to the 1,200-MW PWR plant Biblis-A. Later on, the facility was additionally equipped with a steam generator, plasma-torch aerosol generators, and gas injection systems for air, hydrogen, helium, and carbon dioxide for special investigations. A great flexibility in the model containment geometry could be achieved by:

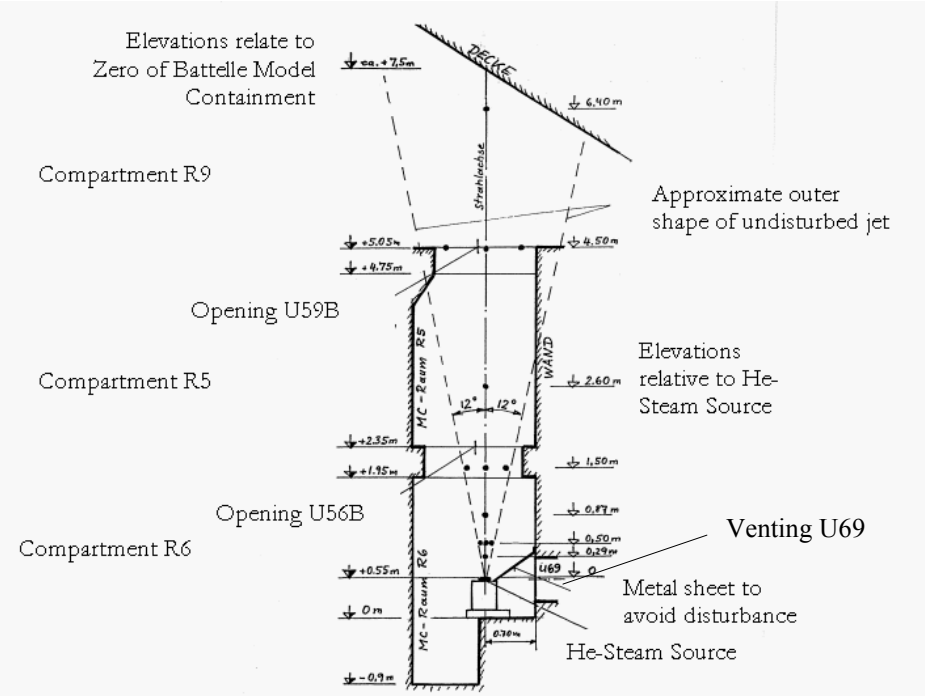

Figure 2 Details of the jet test section inside BMC.

- removable and exchangeable concrete components in the central part of the model containment,
- a surplus of venting openings in the concrete walls between the sub-compartments.

These openings could be partially closed to obtain defined multi-compartment configurations, or let completely open to get a quasi-single-compartment situation, according to the requirements of the particular experiment. In its 23-year operation period (1974-1996) a very large number of different experimental programmes were performed at the BMC facility. Those include:

- LOCA and long-term thermal-hydraulic experiments
- hydrogen distribution, deflagration, and mitigation (HYJET, igniters, recombiners, CO2 dilution) tests
- comprehensive aerosol depletion test programmes (DEMONA, VANAM)

The facility in the configuration used for the HYJET experiments is described in Figure 1 and Figure 2 [Kanzleiter, 1996]. Figure 1 shows the general outline of the BMC. The containment consists of an inner cylindrical room R3 and outer ring room R9 being open at the top to the containments dome area R9. Between R3 and R9 there are the so-called banana-rooms R5 to R8 and the additional room R4. These rooms have connections/openings with each other as well as with R3 and R9. The openings can be closed if desired for the particular experiment. In the HYJET series, room R8 was totally isolated from the other rooms and was therefore not considered in the simulation.

Figure *2* shows a detailed view through the jet release. The jet is directed upwards from the lower part of R6 towards an opening to R5 and the dome R9. The injection-nozzle is shielded by a plate from the junction between R5 and R9.

3. Description of the CFD code

For the benchmark the CFD-Code CFX-5 from ANSYS is used. CFX is a commercial multipurpose CFD code utilized by a large community of CFD users in industry as well in research. As CFX is not restricted to a specific application, it can be also called a multi-physics code. A brief overview of the code is given in the following paragraphs. Further details about the codes can be found in the code handbooks [CFX5.7, 2004].

3.1 CFX-5.7 basics

CFX-5.7 [CFX5.7, 2004] is a 3-D multi purpose code. Meshes of any arbitrary kind of computational cells can be used, such as hexahedral, pyramids, prisms, tetrahedrons and others. CFX-5.7 is a finite volume code based on a coupled solver, which solves the hydrodynamic equations mass, momentum and pressure (u, v, w, p) as a single system. The coupled solver is expected to be faster than the traditional segregated solver of CFX4, since fewer iterations are required to obtain a converged flow solution. For each time-step, the non-linear equations are linearised and assembled into the solution matrix. The linear equations are solved using an Algebraic Multigrid method (Hutchinson and Raithby, 1986). For the time discretisation, a second order backward Euler scheme, that is an implicit time-stepping scheme, was used. The discretisation of the advection term follows a higher order upwind scheme [Barth and Jesperson, 1989]. For modelling of two equation models are used the standard k-ε model and a more advanced SST model [CFX5.7, 2004]. Some details of both turbulence models are described below.

3.2 The k-ε turbulence model

The k-ε model is implemented in many, if not all, general-purpose CFD codes. For real-scale simulations, it has been one of the most used models since it was proven to be stable and numerically robust.

The coupling between the turbulent model and the Reynolds-averaged Navier-Stokes equations comes via the turbulent viscosity. The k–ε model assumes that the turbulent viscosity μ_t is linked to the turbulence kinetic energy k and to the dissipation of turbulence kinetic energy ε via the relation:

$$\mu_{\mathrm{t}} = \frac{C_\mu \rho k^2}{\varepsilon}$$

where ρ is the density. The values of k and ε are directly calculated from the differential transport equations for the turbulence kinetic energy and turbulence dissipation rate:

$$\frac{\partial(\rho k)}{\partial t} + \nabla(\rho U k) = \nabla\left[\left(\mu + \frac{\mu_{\mathrm{t}}}{\sigma_k}\right)\nabla k\right] + P_k - \rho\varepsilon$$

$$\frac{\partial(\rho \varepsilon)}{\partial t} + \nabla(\rho U \varepsilon) = \nabla\left[\left(\mu + \frac{\mu_{\mathrm{t}}}{\sigma_\varepsilon}\right)\nabla \varepsilon\right] + \frac{\varepsilon}{k}(C_{\varepsilon 1} P_k - C_{\varepsilon 2}\rho\varepsilon)$$

where U is the flow velocity vector, t is the time and P_k is the turbulence production due to viscous and buoyancy forces, which is modelled using

$$P_k = \mu_{\mathrm{t}} \nabla U (\nabla U + \nabla U^{\mathrm{T}}) - \tfrac{2}{3}(\nabla U)(3\mu_{\mathrm{t}}\nabla U + \rho k) + P_{k\mathrm{b}}$$

$$\frac{\partial(\rho k)}{\partial t} + \nabla\bullet(\rho \boldsymbol{U} k) = \nabla\bullet\left[\left(\mu + \frac{\mu_t}{\sigma_{k3}}\right)\nabla k\right] + P_k - \beta'\rho k\omega$$

and $C_{\varepsilon 1}$, $C_{\varepsilon 2}$, C_μ as well as σ_k and σ_ε are empirical constants. Standard values can be taken from the literature [Gatski, 1996].

3.3 The SST turbulence model

Although the k–ε turbulence model is widely used it has it has some limitation especially when it comes to complex flows. For this reason a large number of other turbulence models have been developed and implemented in various CFD codes including also CFX. Among those the SST model (**S**hear **S**tress **T**ransport) is the most promising as it combines the advantages of the k-ε turbulence model and of another turbulence model, the baseline (BSL) k-ω model, ω being a turbulent frequency [Menter, 1994]. This is done by using a blending function F_1 that depends on the wall distance and flow conditions. Now the equations for k and ω become:

$$\frac{\partial(\rho k)}{\partial t} + \nabla\bullet(\rho \boldsymbol{U} k) = \nabla\bullet\left[\left(\mu + \frac{\mu_t}{\sigma_{k3}}\right)\nabla k\right] + P_k - \beta'\rho k\omega$$

$$\frac{\partial(\rho \omega)}{\partial t} + \nabla\bullet(\rho \boldsymbol{U} \omega) = \nabla\bullet\left[\left(\mu + \frac{\mu_t}{\sigma_{\omega 3}}\right)\nabla \omega\right] + (1 - F_1)2\rho\frac{1}{\sigma_{\omega 2}\omega}\nabla k\nabla\omega + \alpha_3\frac{\omega}{k}P_k - \beta_3\rho\omega^2$$

and β', α_1, β_1, σ_{k1}, $\sigma_{\omega 1}$, α_2, β_2, σ_{k2}, and $\sigma_{\omega 2}$ are empirical constants. Values can be found in the manual [CFX5.7, 2004]. Nevertheless calculating now the turbulent viscosity from k and ω would over-predict the eddy-viscosity, because this BSL type of formulation would not account for the transport of turbulent shear stresses. Such transport behaviour can be obtained by using a limiter to the kinetic viscosity

$$\nu_t = \frac{a_1 k}{max(a_1\omega, SF_2)}$$

where

$$\nu_t = \mu_t / \rho$$

Again F_2 is a blending function similar to F_1, which restricts the limiter to the wall boundary layer. S is an invariant measure of the strain rate. More details especially on the blending functions F_1 and F_2 can be found in [Menter, 1994] and [CFX5.7, 2004]. At closed boundaries an automatic near-wall treatment is applied.

3.4 Near-Wall treatment

Near wall treatment depends on y^+, a dimensionless distance of the first grid point from the wall. For y^+ the following relations are valid:

$$u^+ = \frac{U_t}{u_\tau} = \frac{1}{\kappa}\ln(y^+)$$

where:

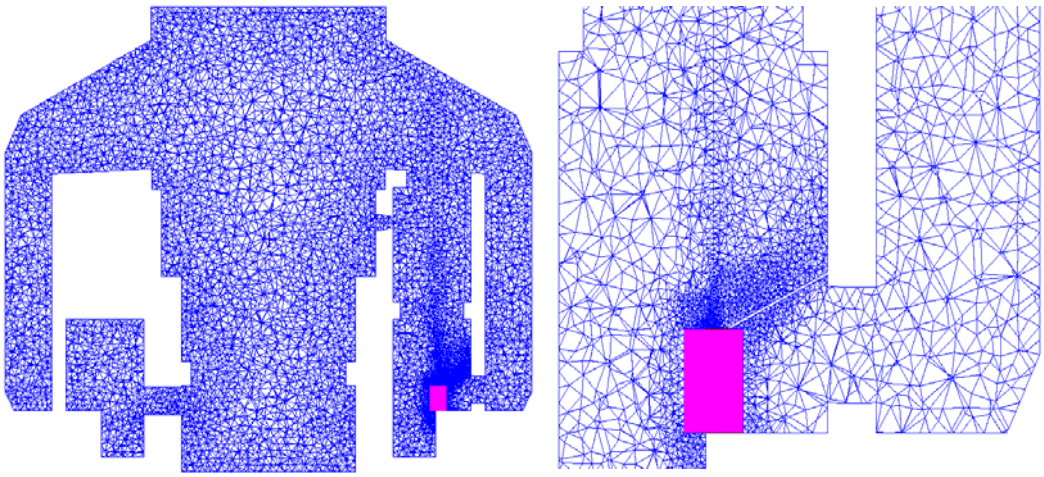

Figure 3: Cut through the BMC displaying the tetrahedral grid (left) and a detail around the nozzle exit (right), where the finest discretization is used.

$$y^+ = \frac{\rho \Delta y u_\tau}{\mu}$$

$$u_\tau = \left(\frac{\tau_\omega}{\rho} \right)^{1/2}$$

u^+ is the near wall velocity, u_τ is the friction velocity, U_t is the known velocity tangent to the wall at a distance of Δy from the wall, τ_ω is the wall shear stress, and κ is the Von Karman constant.

With the k–ε turbulence model scalable wall functions are applied at walls. In this case y^+ should vary between 20 and 100. When the SST turbulence model is used at walls an automatic near-wall treatment is applied. In this case y^+ typically should be below 2. If y^+ values are outside the desired range, a special treatment is applied. This prevents the user from regenerating the grid to adjust y^+ according to the geometrical and flow conditions. More details can be found in [CFX5.7, 2004] and [Menter, 1994].

4. Computational Grids

Two turbulence models (k–ε and SST model) are used on two different grids: a rather standard tetrahedral grid and a finer advanced hybrid grid, where a finer mesh resolution has been employed mainly in the surface normal direction and in the jet region.

4.1 The tetrahedral grid

The grid consists of 1210714 tetrahedral cells or control volumes (CV). The tetrahedral grid is formed by 227737 nodes. Some grid refinement is used in the lower part of the jet region, close to the source of the release. The resolution varies between 4 mm near the inlet nozzle and 0.25 m within the dome of the BMC. The grid and details around the nozzle are shown in Figure 3. Using a pure tetrahedral grid does not allow describing the boundary layers with very much detail compared to a hybrid mesh.

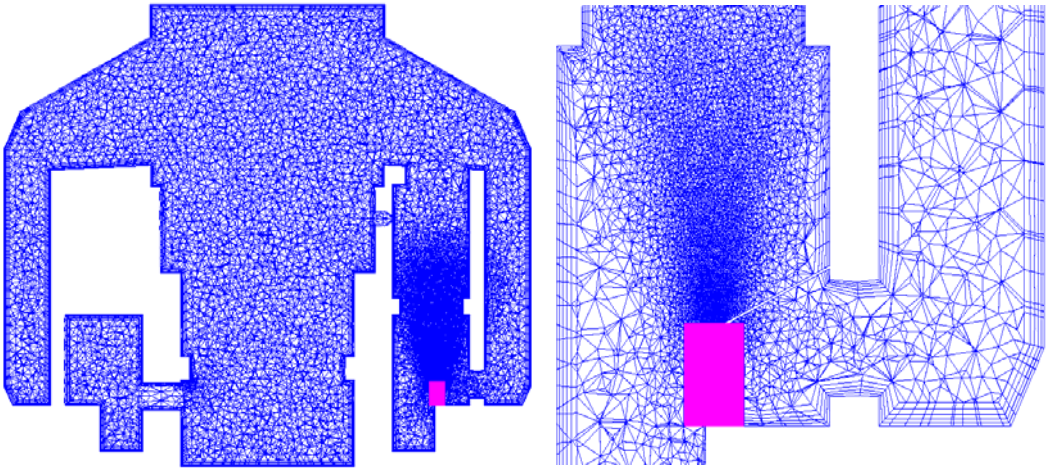

Figure 4: Cut through the BMC displaying the hybrid grid (left) and a detail around the nozzle exit (right), where the finest mesh resolution is used.

On the other hand the mesh generation of a pure tetrahedral grid is more straightforward and simple and it requires typically a smaller number of cells.

4.2 The hybrid grid

As a second grid, a hybrid grid was generated. The grid is composed of 432866 nodes and 1754723 elements (1406277 tetrahedrons, 348256 prisms and 190 pyramids). Starting from a triangular surface grid, prisms are extruded into the volume for a few layers to allow a fine resolution of the boundary layer developing on the wall. Starting from the last prism layer, a tetrahedral grid is filling the larger part of the BMC geometry. Additional grid refinement is used in the lower part of the jet region, close to the source of the release. The grid resolution goes from 2 mm in the regions close to the wall and to the injection, to 0.2 m in regions far from the walls and the injection. The grid and a detail around the nozzle are shown in Figure 4. The fine resolution of the boundary layer in wall normal direction by prism can be seen very well in the detail around the nozzle exit, where the finest discretization is used.

5. Initial Conditions and modelling strategy

Although the experiment was setup to investigate specifically the light-gas release and distribution, heat transfer plays also an important role. Due to the tight time schedule of the experiments, in certain cases the time interval between two experiments was not long enough to prevent that some conditions from the completed experiment could affect the following experiment. Before the HyJet Jx7 experiment, the BMC was used previously for other experiments with also steam involved. At the end of those experiments the concrete structures of the BMC were still at a higher temperature than the ambient temperature. The walls were still cooling down slowly when the HyJet Jx7 experiment was performed. During the cooling down the outer structure cools down faster than the inner structure causing a natural convection loop inside the BMC. Cooler gases are sucked into the inner containment room R3 from the outer ring-room R9. When rising in the inner room R3 to the dome, the gas gets heated from the containment structures. From the dome area the gases fall down into the ring-room R9 where they are cooled down by outer structures, which closes the natural convection loop. Since that convection loop will have a significant effect on the experiment, an initial stationary simulation was performed in order to capture the natural convection loop for both

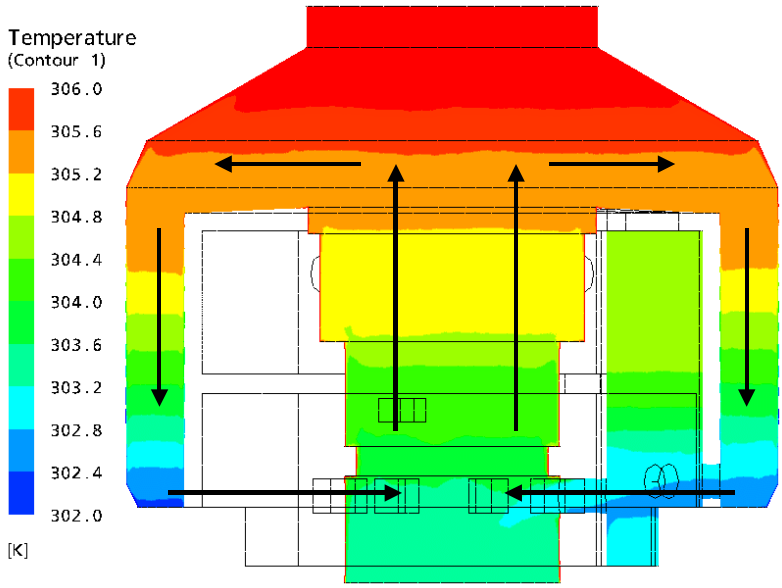

Figure 5: Temperature distribution in the BMC as simulated using the hybrid grid in combination with the SST turbulence model. The arrows show the natural circulation loop.

turbulence models and both grids. The wall temperatures were set accordingly to the values measured in the experiments.

Figure 5 shows the temperature distribution in the BMC as simulated using the hybrid grid in combination with the SST turbulence model, which is in good agreement with measurements (Kanzleiter, 1996). It was possible to predict the temperature distribution and circulation loops accurately only with that combination of grid resolution and turbulence model. The reason is, that the wall functions used in standard k–ε turbulence modelling have limitations in predicting the heat transfer of natural convective flow because the flow and temperature boundary layer is only modelled by wall functions and not simulated, even if a fine boundary layer grid is used. For this reason, when using a k–ε turbulence model a rather coarse grid should be used at the boundary layer. Using the SST turbulence model the flow and temperature distribution in the boundary layer can be simulated but only if the boundary layer is resolved by a fine grid, which is only the case for the hybrid mesh.

Using a hybrid grid in combination with the SST turbulence model, the maximum flow speed due to natural convection goes up to about 0.2 m/s in some areas outside the boundary layer close to hot walls and in some junctions between rooms as can be seen from Figure 6.

Starting from these initial conditions, the release is modelled by applying a constant inlet velocity of 42 m/s (~0.054 Kg/s) of helium for 200 s at the injection inlet. Time integration was done using implicit time-stepping. Although implicit time-stepping should allow the user to set time-step of relatively large size, the time-step had to be defined as rather small (0.05 s) in order to reach the numerical convergency within each time-step within 10 to 20 iterations when using the k–ε turbulence model. When using the SST turbulence model an adaptive procedure was used to define the time step size during the simulation depending on the number of iterations been used for the time-step before. Starting from a small time-step at 0 s, the time-step increased up to 1 s (set maximum) using again typically 10 to 20 iterations per time-step. This was done independent of the grid being used.

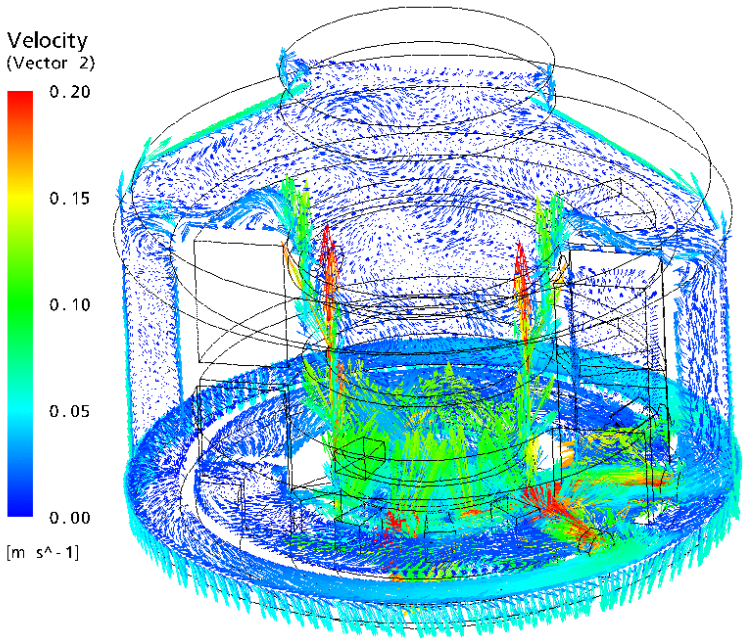

Figure 6: Flow field within the BMC due to natural convection as simulated using the hybrid grid in combination with the SST turbulence model.

Due to the much larger time-step size when the SST turbulence model is used, the computational effectiveness of these simulations is much larger than those done with the k–ε turbulence model. In fact the CPU time used is almost one order of magnitude smaller for the SST than for the k–ε turbulence model. As expected, using the coarser tetrahedral grid also reduces the CPU time by about 50% when using the SST turbulence model and by 30% when using the k–ε turbulence model.

6. Results of the release simulations

In Figure 7 the helium molar fractions within the BMC are shown at four different times during the release and after, in order to illustrate the whole sequence of events – here the SST turbulence model was used in combination with the fine hybrid grid. As can be seen two physical mixing effects can be investigated in the HyJet experiment: small-scale jet entrainment and large-scale stratification.

6.1 The jet behaviour

Figure 8 describes the time history of helium concentration in two positions above the injection nozzle (0.87 m and 2.6 m). The experimental data are shown in comparison with the simulation results of all different types of simulation. Some differences at the beginning and end of the release between experiment and simulations are due to some delay and dilution in the experimental probing system. At 0.87 m height both k–ε turbulence model simulations over-predict the helium concentrations whereas SST turbulence model simulations predict the helium volume concentrations at this position very well. After the release has stopped there is good agreement between experiment and simulations (0% vol. Conc. helium). Due mainly to jet entrainment at the height of 2.6 m above the inlet nozzle, helium volumetric concentration is much lower than at 0.87 m. At this height again both k–ε turbulence model simulations over-predict the helium concentrations whereas SST turbulence model simulations under-predict the helium volume concentrations at this position.

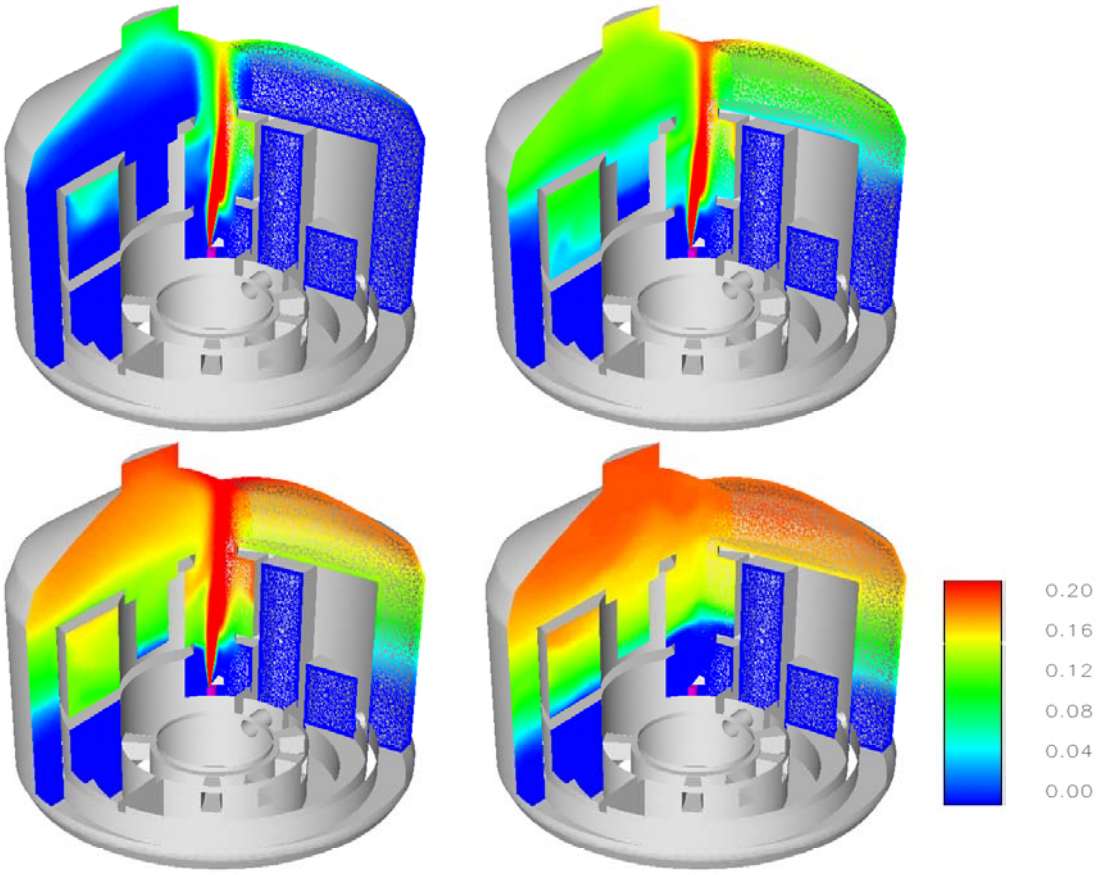

Figure 7: Helium volume concentrations according to legend below at 4 times: 25 s, 100 s, 180 s and 250 s after the release has started (release stops at 200 s) using SST model and hybrid grid.

After the end of the release the helium distribution is determined mainly by stratification. As helium is lighter than air, the higher concentrations of helium can be found close to the ceiling of the dome while the lower concentration are observed close to the bottom of the facility. Therefore at the end of the release, the helium concentration drops to zero at the bottom (and also 0.87 m height) while a higher concentration can be found at 2.6 m due to the stratified atmosphere.

Figure 9 (left) shows a comparison of helium concentrations along the jet axis between experimental data and simulated results after 180 s from the beginning of the release. Due to turbulent jet entrainment, helium concentration decreases from 100% at the nozzle exit to about 20% at the height of 4-5 m. At that height the helium concentration is not only affected by the jet but also by the stratified atmosphere in the BMC. Both Figure 8 and Figure 9 (left) show that some over-prediction occurs especially in the regions closer to the injection when using k–ε turbulence model. With the SST turbulence model, predictions become closer to the experiment. Helium concentration is still slightly over predicted near the nozzle exit and slightly under predicted further downstream. Figure 9 (right) shows horizontal helium concentrations profiles at 1.5 m above nozzle exit. Experimental data is compared with the simulation data. The experimental data indicate that the jet is not axysimmetric, being shifted outwards.

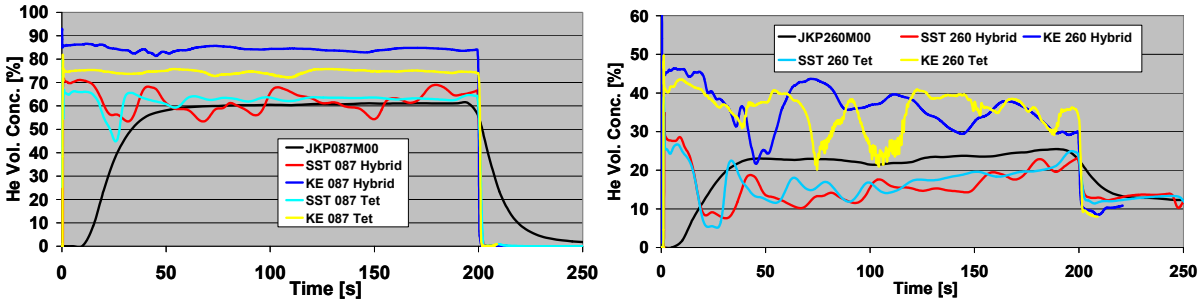

Figure 8: Time history plots of helium volume concentrations at 0.87 m (left) and 2.6 m (right) along the jet axis. Compared are experimental data and simulation results.

This behaviour is due to the shielding plate between opening U69 and the jet nozzle. The flow from the opening is not impinging directly on the jet but it is directed around the jet, giving the jet an outward direction. This behaviour is predicted by all simulations. Helium core concentration is over predicted when the k–ε turbulence model is used. Given the same turbulence model, hybrid grids predict higher core concentration than tetrahedral grids. This could be explained by the fact that the finer grid resolution of the hybrid grid causes less numerical diffusion.

Outside the jet axis the SST turbulence model predicts higher helium concentrations than the k–ε turbulence model (Figure 9 right). This can be explained by larger jet entrainment, which also explains the different behaviour along the jet axis of both turbulence models (Figure 9 left). This is also illustrated in Figure 10. According to Figure 10 the SST model causes much more helium entrainment in the jet than the k–ε model. In addition the jet is more bended outwards (see also Figure 7).

This behaviour corresponds also to the velocity distribution within the jet. Especially data from the k–ε turbulence model using the fine hybrid grid shows strong jet core with only little entrainment, which would cause a reduction in momentum in the jet core but would increase momentum outside the core.

6.2 The behaviour outside the jet and stratification

In Figure 11 the stratification of helium concentration is illustrated. After the release the temperature differences between the outer ring room R9 and the internal rooms R1 – R3 (that was causing natural convection loops before the release Figure 5), is compensated by the higher helium concentrations in the outer ring room R9 than in the internal rooms R1 – R3 at the same height causing all global natural convection loops to stop.

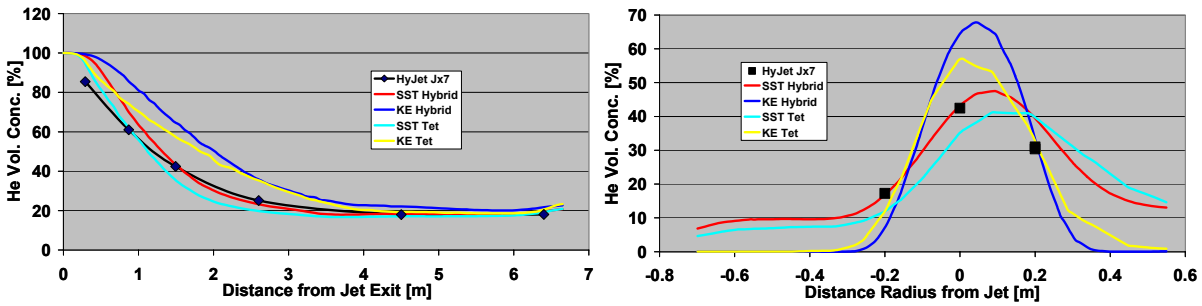

Figure 9: Axial profile (left) through jet axis and horizontal profile (right) of helium volume concentrations through the jet at 1.5 m above the nozzle exit within the opening between R6/R5 both 180 s after the beginning of injection.

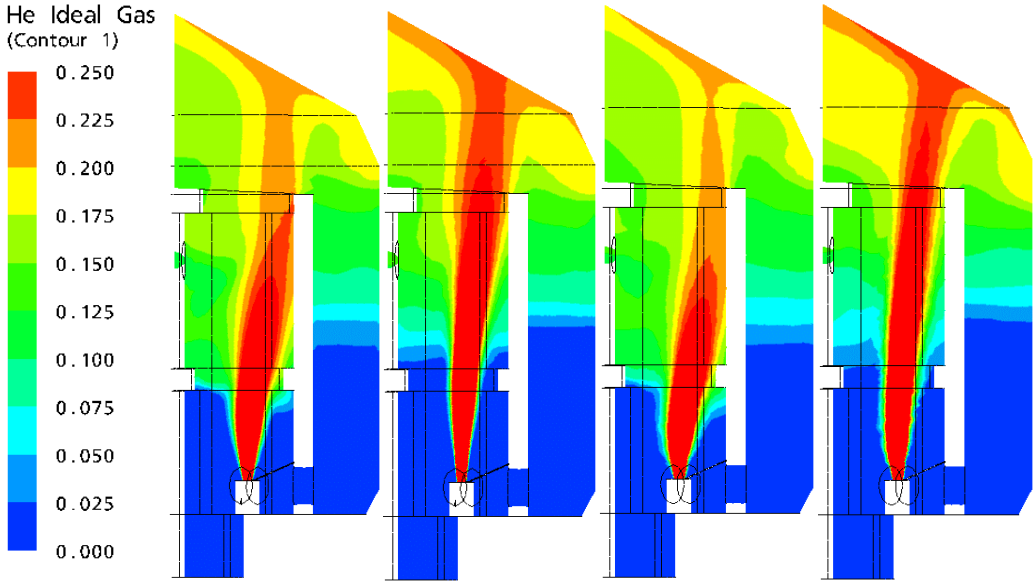

Figure 10: Vertical contour plot through the jet 180 s after release begins. Helium volume concentrations according to legend. From left to right: SST/hybrid grid, k–ε/hybrid grid, SST/tetrahedral grid and k–ε turbulence model /tetrahedral grid.

Figure 12 (left) shows the experimental helium volume concentrations at 6 m height in the centre of the BMC in comparison with simulation results. In all simulations a tendency for over-prediction of helium concentrations occurs. This tendency is stronger in the k–ε turbulence model simulations than in the SST turbulence model simulations. At the beginning of the release also the tetrahedral grid predicts more helium than the hybrid grid. This behaviour could be due to the coarser grid, which causes more numerical diffusion letting the helium cloud arrive earlier at this position.

Figure 12 (right) shows helium volume concentrations along the centre axis of the BMC. Generally in the upper part of the BMC the helium concentrations are more over-predicted for the k–ε than the SST turbulence model simulations. In the lower part of the containment helium concentrations are zero, which is predicted by all simulations. In the interface between zero helium concentration at the bottom and higher concentrations at the top, the stratification layer is a little bit better predicted by the k–ε than the SST turbulence model independently of the grid used. Also the concentration gradient in the stratification layer is larger in the k–ε than the SST turbulence model simulations. This is somewhat supported by the experimental measurements.

The little differences between the results of the k–ε and the SST turbulence model simulation can be explained by the fact that for free shear flows, the SST turbulence model is identical to the k–ε turbulence model. Therefore for large parts of the HyJet simulations, both models are the same, except close to the boundary and in the jet, which again is consistent with what has been observed within section 5 and 6.1.

7 Conclusions

The CFD code CFX-5.7 was validated against experimental data for a helium jet release and dispersion case. Two different turbulence models (k-ε and SST turbulence model) were used with two different grid approaches, a pure tetrahedral grid and a hybrid grid. From the quantitative point of view, the agreement between experimental data and simulation results is satisfactory but not always

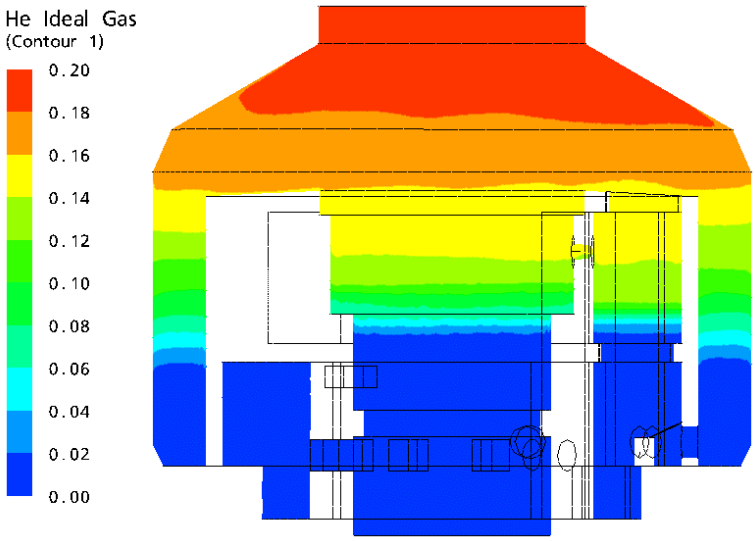

Figure 11: Stratified helium atmosphere 200 s after the release has stopped. The picture was extracted from a simulation using the hybrid grid in combination with the SST turbulence model.

excellent. Some level of over prediction for the helium concentration was observed, especially in regions close to the nozzle exit and in the upper part of the BMC.

The SST turbulence model was capable of providing better predictions than the standard k-ε turbulence model, especially in regions within the jet. Moreover the better numerical effectiveness of the SST turbulence model was proven, since the calculations with the SST model were almost one order of magnitude faster in computation time than the computations with the k-ε model.

The hybrid grid was to be preferred when combined with the SST turbulence model. The fine boundary layer grid allowed much better predictions of the heat transfer to the wall. This will become even more relevant when wall condensation and evaporation have to be considered. This easily justifies the extra computational cost been involved with such a grid approach. It should also be mentioned that generating a hybrid grid could be much more labour intensive than using just a pure tetrahedral grid. New advanced automatic grid generation techniques might overcome this problem in the future.

Although the k-ε model is the most commonly used turbulence model in most CFD applications, it does not provide very accurate predictions for this application. Alternatively the SST turbulence model was employed giving more accurate results. One of the reasons of the better predictions of the SST model compared to the k-ε model has been identified in the coupling between the turbulent model and the grid resolution close to the wall. This investigation provided a confirmation that the validation of commercial CFD codes is required in order to select the more suitable physical models and computational grids for each specific application and in order to evaluate the accuracy of the predictions.

Future work should include a larger number of physical phenomena that have an effect on hydrogen distribution during jet release and gas-dispersion such as the conjugate heat transfer that is the heat transfer through the walls. Other physical effects to be considered are two phase flow, including wall condensation and evaporation, sprays and the coupling between autocatalytic recombiners and the convective flow that they could drive within the containment.

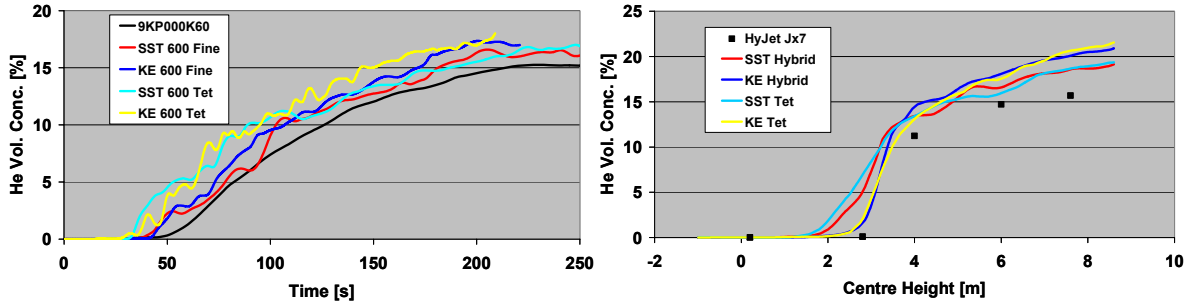

Figure 12: Time history plots at 6 m height (left) and a axial profile of helium volume concentrations at 205 s – 5 s after release stopped - in the centre axis of the BMC.

Acknowledgements

The authors would like to thank Teja Kanzleiter and his team from Becker Technologies who performed the experiments and who kindly provided the experimental data in digital format.

This work was partially sponsored by the European Network of Excellence SARNET, Contract FI6O-CT-2004-509065.

References

Barth, T.J., and Jesperson, D.C., 1989, The design and application of upwind schemes on unstructured meshes. *AIAA Paper* 89-0366.

CFX-5.7, 2004, *User Documentation*, ANSYS Inc, USA.

DoE 2002, , A National vision of America's transition to a Hydrogen economy – To 2030 and beyond, *US Department of Energy Report* .

Fire and Explosion Guidance, Part 1. Oct 2003, HSE and UKOOA, Uk Offshore Operators Association Publisher.

Gastski, T. B. 1996 Turbulent flows: model equations and solution methodology. In *Handbook of Computational Fluid Mechanics*, Peyret, R. (Ed.), Academic Press, London.

Hutchinson, B.R. and Raithby, G.D., 1986, A Multigrid method Based on the Additive Correction Strategy, *Numerical Heat Transfer*, Vol. 9, pp. 511-537.

Kanzleiter T., 1996, HYJET-PACOS-Versuche im Modellcontainment, *Abschlussbericht BF-R40.075-10*, Batelle Institute, Eshborn, Germany.

Menter, F.R., 1994, Two-equation eddy-viscosity turbulence models for engineering applications, AIAA-Journal, 32(8)